



Triple oxygen and multiple sulfur isotope constraints on the evolution of the post-Marinoan sulfur cycle

Peter W. Crockford^{a,*}, Benjamin R. Cowie^{b,1}, David T. Johnston^b, Paul F. Hoffman^{b,d}, Ichiko Sugiyama^a, Andre Pellerin^a, Thi Hao Bui^a, Justin Hayles^c, Galen P. Halverson^a, Francis A. Macdonald^b, Boswell A. Wing^a

^a McGill University and GEOTOP, 3450, University Street, Montreal, Quebec, H3A 0E8 Canada

^b Harvard University, 20, Oxford Street, Cambridge, MA 02138, United States

^c Louisiana State University, Howe Russell Kniffen, Baton Rouge, LA 70803, United States

^d University of Victoria, 3800, Finnerty Road (Ring Road), Victoria, BC, V8P 5C2, Canada



ARTICLE INFO

Article history:

Received 28 October 2014

Received in revised form 20 October 2015

Accepted 16 December 2015

Available online xxxx

Editor: G.M. Henderson

Keywords:

triple oxygen

barite

sulfur cycle

Neoproterozoic

cap dolostone

snowball earth

ABSTRACT

Triple oxygen isotopes within post-Marinoan barites have played an integral role in our understanding of Cryogenian glaciations. Reports of anomalous $\Delta^{17}\text{O}$ values within cap carbonate hosted barites however have remained restricted to South China and Mauritania. Here we extend the $\Delta^{17}\text{O}$ anomaly to northwest Canada with our new measurements of barites from the Ravensthrone cap dolostone with a minimum $\Delta^{17}\text{O}$ value of $-0.75\text{\textperthousand}$. For the first time we pair triple oxygen with multiple sulfur isotopic data as a tool to identify the key processes that controlled the post-Marinoan sulfur cycle. We argue using a dynamic 1-box model that the observed isotopic trends both in northwest Canada and South China can be explained through the interplay between sulfide weathering, microbial sulfur cycling and pyrite burial. An important outcome of this study is a new constraint placed on the size of the post-Marinoan sulfate reservoir ($\approx 0.1\%$ modern), with a maximum concentration of less than 10% modern. Through conservative estimates of sulfate fluxes from sulfide weathering and under a small initial sulfate reservoir, we suggest that observed isotopic trends are the product of a dynamic sulfur cycle that saw both the addition and removal of the $\Delta^{17}\text{O}$ anomaly over four to five turnovers of the post-Marinoan marine sulfate reservoir.

© 2015 Elsevier B.V. All rights reserved.

1. Introduction

The dramatic climate transition observed at the boundary between the Cryogenian and Ediacaran periods (635 Ma) is well documented but poorly understood. The Snowball Earth Hypothesis postulates that during this transition, Earth's oceans were frozen in a runaway ice-albedo feedback that was finally disrupted by the gradual, syn-glacial build-up of volcanicogenic greenhouse gases (primarily CO_2) in Earth's atmosphere (Hoffman et al., 1998). The Snowball Earth event at the end of the Cryogenian period (the 635 Ma Marinoan glaciation) is marked by "cap carbonate" deposits and, in several regions of the world, thin intervals of barite (BaSO_4) (Hoffman et al., 2011; Macdonald et al., 2013). The recent discovery of large deficits in ^{17}O – ^{16}O ratios, relative to those expected from the ^{18}O – ^{16}O ratios in Snowball-associated barites,

has drawn new attention to these deposits (Bao et al., 2008; Peng et al., 2011).

Stratospheric production of ozone preferentially concentrates the heavy oxygen isotopes (^{17}O and ^{18}O) in equal proportions relative to their lighter counterpart (^{16}O) (Thiemens and Heidenreich, 1983), and isotopic exchange results in the enrichment of stratospheric gases, principally CO_2 , in the two heavy isotopes of oxygen (Yung et al., 1991, 1997). Conversely, stratospheric O_2 bears the isotopically lighter fraction, and is anomalously enriched in ^{16}O , and depleted in ^{17}O (Luz et al., 1999). This stratospheric isotopic anomaly is mixed into the tropospheric O_2 reservoir, where it can lead to ^{17}O depletions in tropospheric O_2 . These ^{17}O depletions are tempered in the troposphere by O_2 generated through oxygenic photosynthesis (Luz et al., 1999), which is sourced ultimately from the hydrosphere and carries no mass-independent ^{17}O anomaly. Mass exchange between the stratosphere–troposphere seems to be relatively insensitive to changing atmospheric compositions (Butchart et al., 2006), therefore, the unique oxygen isotope signatures in post-Marinoan barites likely reflect perturbations to

* Corresponding author. Tel.: +1 514 995 4397.

E-mail address: peter.crockford@mail.mcgill.ca (P.W. Crockford).

¹ Both authors contributed equally to this work.

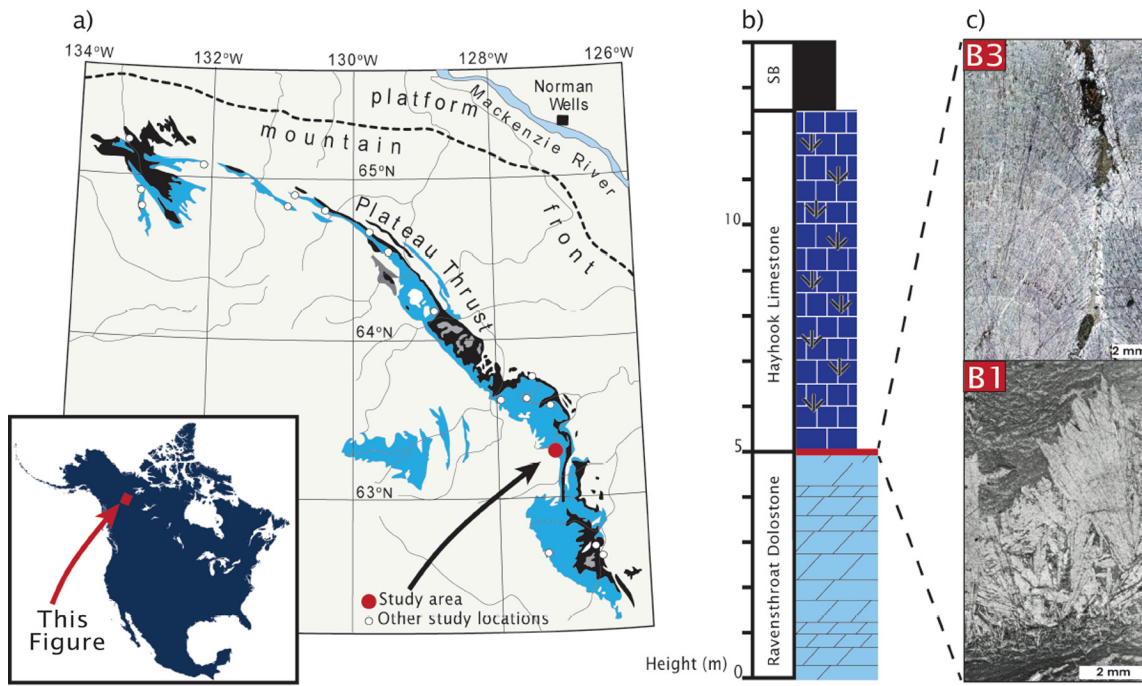


Fig. 1. (a) Exposed Neoproterozoic stratigraphy in the Mackenzie Mountains in northwest Canada where barites from this study were sampled. (b) Stratigraphic log outlining barite occurrence at the top of the Ravensthorpe cap dolomite, underlying the Hayhook Limestone. (c) Digital photomicrographs of barite fans taken in unpolarized light in ~ 3 mm-thick polished thin sections, where examples of the change in textures observed in the barite unit are observed with basal bladed crystal fans in the B1 horizon and digitate groups with widely spaced laminations in the B3 horizon.

either biospheric productivity (Sansjoefre et al., 2011), atmospheric CO₂ levels (Bao et al., 2008), or possibly both (Cao and Bao, 2013; Wing, 2013).

Transfer of the atmospheric isotope signal to marine sulfate starts with oxidative weathering of sulfide minerals, producing aqueous sulfate with up to 25% of its oxygen from tropospheric O₂ (Balci et al., 2007; Bao et al., 2008; Kohl and Bao, 2011). Rivers transport this sulfate to the oceans where it, and the isotopic anomaly it carries, is diluted into the standing stock of marine sulfate. Sulfate also fuels microbial sulfur cycling (MSC) in marine environments. The sulfide produced along the reductive branch of MSC can be re-oxidized to sulfate (Jørgensen, 1990), leading to a flux of isotopically normal ($\Delta^{17}\text{O} = 0$) sulfate back into the marine pool (Peng et al., 2011). This same set of processes (sulfide weathering and MSC) carry sulfur isotope consequences for the marine sulfate reservoir, mediated by the fraction of sulfur that leaves the marine environment through pyrite burial. The sulfide produced from sulfate reduction will be enriched in ³²S, leaving a sulfate counterpart that is enriched in ³⁴S. As preserved in the sedimentary record, sulfur isotopic differences between sulfates and sulfides are related to both oceanic sulfate concentrations (Gomes and Hurtgen, 2015; Bradley et al., 2016) and organic carbon availability, as manifest through sulfate reduction rates in marine sediments (Leavitt et al., 2013). Re-oxidative sulfur cycling can amplify this isotopic difference between reduced and oxidized forms of sulfur (Canfield and Thamdrup, 1994) but it also produces characteristic ^{33}S – ^{32}S fractionations that enable it to be distinguished from MSC's reductive branch (Johnston et al., 2005; Pellerin et al., 2015a; Wu et al., 2010). Coupled oxygen and sulfur isotope measurements from post-Marinoan barite, therefore, are a potentially powerful tool to resolve not only atmospheric compositions, but also the dominant metabolic contributions and critical fluxes into and out of the marine reservoir during this unique time in Earth history.

Although considerable attention has been given to the dynamics of the sulfur cycle across the Cryogenian–Ediacaran transition,

many outstanding questions remain. For example, the initial size of the marine sulfate reservoir at the end of the Marinoan glacial episode, and the rapidity of its growth to typical Phanerozoic levels is still unknown. Sulfur isotope fractionations between sulfate and sulfide in different post-Marinoan sedimentary packages have been used to argue for an initial sulfate reservoir of late Archean proportions that grew to Phanerozoic levels over ≈ 30 million years (Halverson and Hurtgen, 2007). Alternatively, large depletions in ³⁴S in sulfides from black shales have been interpreted to reflect a more immediate oxidative response, with the growth of a sizable sulfate reservoir occurring at a rate that was more than an order of magnitude more rapid (Sahoo et al., 2012). The microbial dynamics of the sulfur cycle over this interval are also uncertain, with the suggestion of a broad interval of enhanced re-oxidative sulfur cycling preceding the Marinoan glacial interval (Canfield and Teske, 1996) as well as a vigorous oxidative component of MSC drawing down marine sulfate levels in the earliest Ediacaran (Peng et al., 2011). Given the complicated relationship between atmospheric oxygen, marine sulfate levels, and the intensity of microbial sulfur re-oxidation, these conflicting results make it difficult to reconstruct the nature of the ocean – atmosphere system in the aftermath of the Marinoan glaciation.

In this study we provide new data and interpretation of the post-Marinoan sulfur cycle through the isotopic record within barite fans from the Mackenzie Mountains in northwest Canada (Fig. 1). This dataset includes the first paired triple oxygen and multiple sulfur isotope measurements from a Marinoan-aged barite. These data are interpreted within a time-dependent model of post-glacial sulfate cycling to explain observed isotopic trends and the environmental conditions accompanying barite deposition. By extending the record of the ¹⁷O anomaly in barite to another paleo-continent, we link these isotopic shifts to the global operation of the post-Marinoan sulfur cycle. Through this approach we make new estimates for the size of the post-Marinoan sulfate reservoir and the impact of re-oxidative sulfur cycling. These

results provide model-dependent estimates for the time interval captured by both barite units and underlying cap carbonates.

2. Materials and methods

2.1. Sample description

Two predominant morphologies of macroscopic barite occur in Marinoan cap dolostones worldwide. The first type is diagenetic, forming void filling crustose cements ([Shields et al., 2007](#)) and tepee-like breccias interpreted as subaqueous ([Jiang et al., 2006](#)) or vadose ([Zhou et al., 2010](#)) in origin. The second type – seafloor barite fans – are primary and abiogenic. These barite fans grew directly into the water column, and they are preserved within an iron and manganese-rich dolomitic matrix. Seafloor barite structures are found above or within cap dolostone units commonly below buildups of aragonite fans ([Hoffman et al., 2011](#)).

Seafloor barite is the primary barite morphology observed in the Ravensthrat Formation cap dolostone in the southern and central portions of the Mackenzie Mountains in the northern Canadian Cordillera ([Hoffman et al., 2011; Macdonald et al., 2013](#)) ([Fig. 1](#)). The geological and chemostratigraphic succession in the Mackenzie Mountains is similar to other cap carbonate successions elsewhere, representing a transgressive sequence with large negative shifts in carbon isotope ratios occurring at the top of the cap dolostone unit ([Hoffman and Halverson, 2011](#)).

Barite layers in the Ravensthrat Formation immediately overlying the cap dolostone, are typically 4–10 cm thick, and consist of bladed crystals and upward-fanning rosettes ([Fig. 1c](#)). The upward-oriented growth habit, sediment drape that thins over crystal terminations, and presence of crystal fragments as detrital material within the sediment matrix indicate the barite was deposited at the sediment-water interface. Importantly, there are three distinct generations of barite that were sequentially deposited at the top of the Ravensthrat Formation ([Fig. 1](#)). The first generation structures (Type B1) are 1–2 cm in height and consist of fine fans of barite blades originating from common nucleation centers and draped with laminated peloidal Fe-rich dolomite sediment ([Arnaud et al., 2011](#)) ([Fig. 1c](#)). The B1 structures are covered by larger (2–3 cm) internally laminated fans and rosettes (Type B2) interspersed within the dolomite matrix. The uppermost barite structures (Type B3) are even larger (3–4 cm) and consist of fans that have coalesced into digitate groups with more widely spaced internal laminations. These latest formed barites are inclusion rich, and have thin rinds of inclusion-free barite separated by Fe-rich sediment infill ([Fig. 1c](#)). The preservation of these delicate textures, together with systematic isotopic trends identified here, suggest that barites from northwest Canada have not been affected by any post-depositional geochemical modification. The occurrence of equivalent units on four other paleo-continents ([Kennedy, 1996; Bao et al., 2008; Hoffman et al., 2011](#)) suggests global similarity of depositional processes and timing among the Marinoan seafloor barite units.

2.2. Oxygen isotope measurements

Triple oxygen isotope measurements followed the methods detailed by [Bao et al. \(2008\)](#). Barite powders were dissolved and re-precipitated as pure barite via a modified DTPA (diethylenetriaminepentaacetic acid) procedure to remove any potential contamination from non-sulfate bearing minerals ([Bao, 2006](#)). This involved first dissolving the samples in a 0.05 M DTPA, 0.1 M NaOH solution over 12 h in a sample shaker. Samples were subsequently acidified with 6 M HCl in a water bath at 80 °C to drive off any CO₂, thereby preventing the formation of witherite during the re-precipitation of barite ([Bao and Thiemens, 2000](#)). Pyrite oxidation

was not a large concern in contamination of samples since pyrite abundance was determined through high-resolution micrographs, and determined to be a maximum concentration of 0.5% within the micrite phase. Samples were then loaded onto a stainless steel stage and placed under a BrF₅ atmosphere for 12 h to react with any trace water in the samples. Oxygen gas was generated with a CO₂-laser fluorination system on approximately 10 mg of sample powder. Typical yields of O_{2(g)} were between 25–35% on the barite sample powder, resulting in approximately 25 μmol of O_{2(g)} for analysis. Triple oxygen isotope compositions of O₂ derived from barite were measured on a Thermo MAT 253 in dual-inlet mode in the OASIC laboratory at Louisiana State University, and are expressed as:

$$\Delta^{17}\text{O} = \delta'^{17}\text{O} - 0.52 \times \delta'^{18}\text{O} \quad (1)$$

where, $\delta'^i\text{O} = \ln(iR_{\text{sample}}/iR_{\text{SMOW}}) \times 1000$, $iR = {}^i\text{O}/{}^{16}\text{O}$ and i is 17 and 18. Results are presented on the SMOW scale (cf. [Bao et al., 2008](#)). Repeat measurements on pure BaSO₄ laboratory standards yielded a 1σ analytical uncertainty for Δ¹⁷O measurements of less than 0.05‰.

Microdrilled barite powders were also analyzed for their δ¹⁸O values via a TC/EA coupled to a Thermo Delta V configured in continuous flow mode at Harvard University. Each sample was run in duplicate, with an established standard deviation of 0.3‰ (1σ) for replicate analyses of in-house standards. The composition of unknowns was calibrated against international standards (IAEA SO5, IAEA SO6, and NBS-127) that were interspersed through each run (see [Johnston et al., 2014](#) for additional detail). Values are expressed as:

$$\delta^{18}\text{O} = ({}^{18}R_{\text{sample}}/R_{\text{standard}}) \times 1000 \quad (2)$$

where ${}^{18}R = {}^{18}\text{O}/{}^{16}\text{O}$.

2.3. Sulfur isotope measurements

Multiple sulfur isotope measurements ($\delta^{34}\text{S}$, $\Delta^{33}\text{S}$, $\Delta^{36}\text{S}$ values) were performed by reacting powdered barite samples first in a boiling Cr-reducing solution ([Canfield et al., 1986](#)), which liberated minor H₂S from trace sulfides in the barite. Modal analysis showed that these sulfides always formed less than 0.3 mol% of the sulfur in a given sample. The resulting powders were then rinsed repeatedly with Milli-Q H₂O and dried over night. To measure the isotopic composition of the sulfates approximately 10 mg of the dried powder was then reacted with 15 mL of Thode reduction solution at 100 °C ([Thode et al., 1961](#)), which converts sulfate to H₂S. Hydrogen sulfide gas was carried through a N₂ gas stream and was bubbled through a Zn acetate solution where it was converted to ZnS. Samples were then precipitated as Ag₂S after reaction with 0.2 M AgNO₃. Dried Ag₂S samples were reacted with F_{2(g)} in nickel bombs at 250 °C, to generate pure SF_{6(g)}. The isotopic composition of SF_{6(g)} was first purified via gas chromatography and analyzed on a Thermo MAT-253 in dual inlet mode in the Stable Isotope Laboratory at McGill University. Results were normalized to repeated measurements of international reference material IAEA-S-1, with a defined $\delta^{34}\text{S}$ value of −0.3‰ on the Vienna Canyon Diablo Troilite (V-CDT) scale. We took the $\delta^{33}\text{S}$ value of IAEA-S-1 to be −0.061‰ V-CDT. Sulfur isotope compositions are expressed as:

$$\delta^i\text{S} = ([{}^iR_{\text{sample}}/{}^iR_{\text{V-CDT}}] - 1) \times 1000 \quad (3)$$

where ${}^iR = {}^i\text{S}/{}^{32}\text{S}$ and i is 33, 34, or 36, and

$$\Delta^i\text{S} = \delta^i\text{S} - 1000 \times ([1 + (\delta^{34}\text{S}/1000)]^{i\lambda} - 1) \quad (4)$$

where i is 33 or 36. We calculated $\Delta^{33}\text{S}$ and $\Delta^{36}\text{S}$ values through reference mass dependent exponents, of ${}^{33}\lambda = 0.515$, and

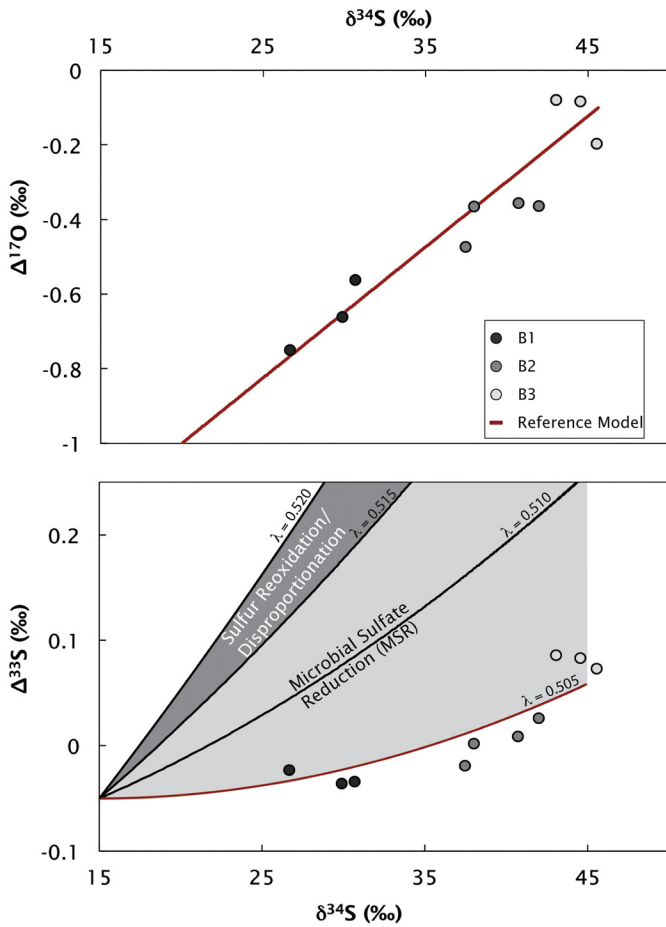


Fig. 2. (a) Ravensthorpe formation barite $\Delta^{17}\text{O}$ and $\delta^{34}\text{S}$ data plotted on the reference model solution (${}^{34}\varepsilon = -42$ and $f_{\text{py}} = 0.95$) for sulfate isotope values. (b) Ravensthorpe formation barite $\Delta^{33}\text{S}$ and $\delta^{34}\text{S}$ data plotted on reference model solution for sulfate isotope values calculated for varying values of ${}^{33}\lambda$. Total analytical uncertainty is estimated to be: $\Delta^{17}\text{O}$ (1σ analytical uncertainty = 0.05‰), $\delta^{34}\text{S}$ (1σ analytical uncertainty < 0.1‰), and $\Delta^{33}\text{S}$ (1σ analytical uncertainty < 0.01‰).

${}^{36}\lambda = 1.9$, representative of equilibrium sulfur isotope exchange at high temperatures. Uncertainty (1σ) on the entire analytical procedure is estimated to be better than 0.1‰ for $\delta^{34}\text{S}$, 0.01‰ for $\Delta^{33}\text{S}$ and 0.2‰ for $\Delta^{36}\text{S}$.

3. Results

The sequential nature of three barite textures allows geochemical signatures to be placed in relative chronological order. Values of $\Delta^{17}\text{O}$, $\delta^{18}\text{O}$, $\delta^{34}\text{S}$, and $\Delta^{33}\text{S}$ all show clear trends with the progression from the earliest formed barite (B1) to the latest (B3) (Fig. 2). Type B1 captures the largest negative $\Delta^{17}\text{O}$ values and lightest $\delta^{18}\text{O}$ values with a mean value of -0.66‰ and 17.95‰ respectively. In the later formed type B3 barite, the $\Delta^{17}\text{O}$ signal is diminished and $\delta^{18}\text{O}$ values progressively heavier, reaching -0.12‰ and 19.51‰ respectively (Fig. 2a; Table 1). Similar isotopic trends were observed in sulfur data that showed a mean $\delta^{34}\text{S}$ value of 29.5‰ , and a $\Delta^{33}\text{S}$ value of $\approx -0.04\text{‰}$. The $\delta^{34}\text{S}$ and $\Delta^{33}\text{S}$ values increase reaching averages of 45‰ and 0.08‰ respectively for type B3 (Fig. 2b; Table 1). These observations suggest that the seafloor barite horizon was sourced from a sulfate pool with an evolving isotopic composition. In the analysis that follows, we take the near linear positive covariation of $\Delta^{17}\text{O}$ and $\delta^{34}\text{S}$ as the primary geochemical signal to be modeled, and reserve the positive covariation of $\Delta^{33}\text{S}$ with $\delta^{34}\text{S}$ as an independent test of the model predictions.

Table 1

$\Delta^{17}\text{O}$ (1σ analytical uncertainty = 0.05‰), $\delta^{34}\text{S}$ (1σ analytical uncertainty < 0.1‰), $\Delta^{33}\text{S}$ (1σ analytical uncertainty < 0.01‰), and $\Delta^{36}\text{S}$ (1σ analytical uncertainty < 0.2‰) stable isotope ratios for Types B1, B2 and B3 barite textures from NW Canada. Analyses of barites for $\delta^{18}\text{O}$ represent micro-drilled sub samples of individual barite layers (NM = not measured).

Sample	$\Delta^{17}\text{O}$	$\delta^{18}\text{O}$	$\delta^{34}\text{S}$	$\Delta^{33}\text{S}$	$\Delta^{36}\text{S}$	Texture
2-1	-0.75	18.77	26.66	-0.023	-0.62	B1
2-2	-0.66	17.12	29.89	-0.036	-0.67	B1
2-4	-0.56	NM	30.82	-0.037	-0.75	B1
4-1	-0.36	18.33	40.70	0.009	-0.51	B2
4-2	-0.36	18.98	41.98	0.026	-0.64	B2
4-3	-0.37	NM	37.99	0.002	-0.99	B2
4-4	-0.47	NM	37.45	-0.019	-0.09	B2
3-1	-0.20	19.51	45.53	0.073	-0.16	B3
3-2	-0.08	19.78	43.04	0.086	-0.29	B3
3-3	-0.08	19.25	44.54	0.083	0.32	B3

4. Discussion

4.1. Existing interpretations of the isotopic evolution of post-Marinoan seafloor barite

There are three published models for the sulfur and/or oxygen isotope evolution of post-Marinoan barites. One conceptual model for barite deposition called on the upwelling of anoxic barium- and sulfate-rich but sulfate-poor deep waters into an oxygenated surface ocean (Hurtgen et al., 2006). Upon mixing of these two water masses, aqueous sulfide would have been oxidized, providing a $\delta^{34}\text{S}$ -depleted source of sulfate and driving barite supersaturation (Hurtgen et al., 2006). This type of sulfide oxidation would deposit sulfate with the $\Delta^{17}\text{O}$ of ocean water ($\Delta^{17}\text{O} \approx 0\text{‰}$ VSMOW), leading either to negative covariation between $\delta^{34}\text{S}$ and $\Delta^{17}\text{O}$ or a wide range of $\delta^{34}\text{S}$ at a $\Delta^{17}\text{O} \approx 0\text{‰}$ (cf. carbonate-associated sulfate from W2 dolomites of Bao et al., 2009). However, we observe a positive correlation between $\delta^{34}\text{S}$ and $\Delta^{17}\text{O}$ and significantly non-zero $\Delta^{17}\text{O}$, suggesting that an alternative process is required for the barites reported here (Table 1) and elsewhere (Bao et al., 2008; Peng et al., 2011).

A second conceptual model associates the formation of Marinoan-age void-filling barite cements and crusts with the deposition of barite in methane-rich cold seeps on the modern day seafloor (Shields et al., 2007). Modern cold-seep barite is spatially localized with a wide range of $\delta^{34}\text{S}$ values that do not follow a coherent stratigraphic order (Torres et al., 2003). In contrast, the Ravensthorpe barite layer has a broad spatial distribution, and exhibits a monotonic stratigraphic variation of $\delta^{34}\text{S}$ values (Table 1; Fig. 2). Although modern cold seeps appear to encompass a similar range in $\delta^{34}\text{S}$ values, $\delta^{18}\text{O}$ values from the Ravensthorpe barite plot in a much more limited range (Table 1). Therefore this places the Ravensthorpe barites on a very different $\delta^{18}\text{O}$ - $\delta^{34}\text{S}$ trend than these previously suggested modern analogues (Shields et al., 2007; Antler et al., 2015). These observations suggest that an actualistic interpretation based on modern cold seep barites is not appropriate for the barites studied here.

Finally, a third coupled $\Delta^{17}\text{O}$ and $\delta^{34}\text{S}$ record in Marinoan barite from South China has been quantitatively reproduced in a model of the sulfur cycle after a Snowball Earth (Peng et al., 2011). This model starts with a standing pool of isotopically anomalous sulfate in the post-glacial ocean. It requires intense microbial sulfate reduction (MSR) to drive sulfate $\delta^{34}\text{S}$ to more positive values, and nearly equally intense re-oxidation of the sulfide to reset sulfate $\Delta^{17}\text{O}$ toward a value of 0‰ (Peng et al., 2011). Importantly the model can only generate a positive covariation between $\delta^{34}\text{S}$ and $\Delta^{17}\text{O}$ if no sulfate is supplied to the ocean through oxidative weathering of continental rocks or sediments. Consumption of a “closed” sulfate reservoir by net sulfate reduction leads to continually increasing $\delta^{34}\text{S}$ values through a continual decline of the

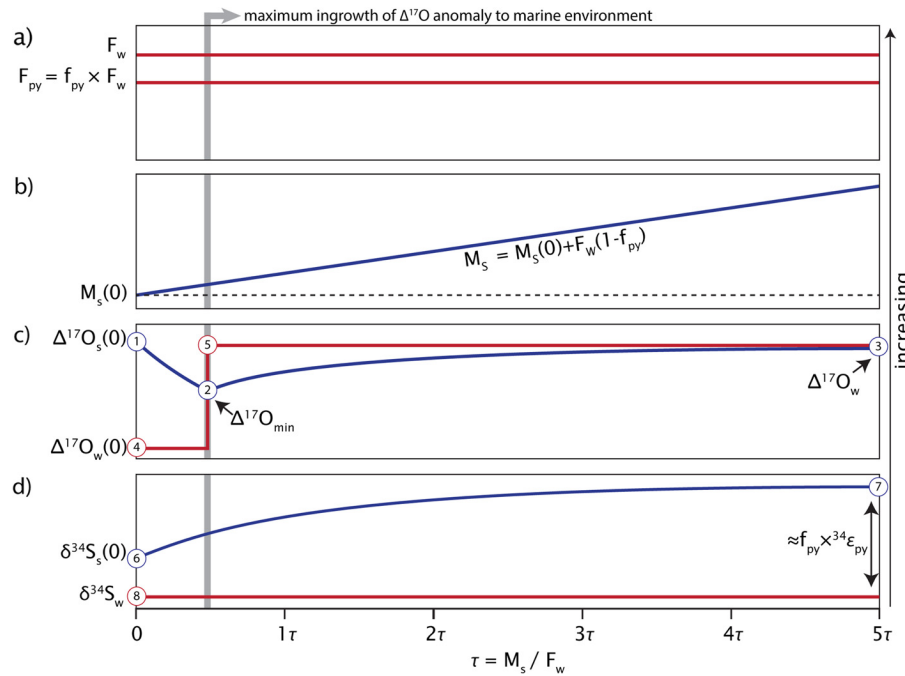


Fig. 3. Qualitative description of reference model forcing and responses: f_{py} , F_W , $\Delta^{17}\text{O}_W$, $\delta^{34}\text{S}_W$ and M_s , $\Delta^{17}\text{O}_s$, $\delta^{34}\text{S}_s$ over five turnover periods (τ) of the marine sulfate reservoir. Model forcing is shown in red, while responses are shown in blue and the critical transition in F_W when the maximum $\Delta^{17}\text{O}$ anomaly is imparted to the marine environment is marked with the grey line. Numerical values are not assigned along y-axes, however increases in vertical height correspond to increasing values. Circles filled with numbers 1–8 correspond to reference model values, as set by observations (1: initial marine $\Delta^{17}\text{O}$ value = $-0.1\text{\textperthousand}$, 2: minimum marine $\Delta^{17}\text{O}$ value = $-1\text{\textperthousand}$, 3: $\Delta^{17}\text{O}$ marine at isotopic steady-state = $-0.1\text{\textperthousand}$, 4: initial $\Delta^{17}\text{O}$ value of weathering flux = $-4.2\text{\textperthousand}$, 5: $\Delta^{17}\text{O}$ value of weathering flux after maximum marine anomaly is reached = $-0.1\text{\textperthousand}$, 6: initial marine $\delta^{34}\text{S}$ value = $+15\text{\textperthousand}$, 7: $\delta^{34}\text{S}$ marine at isotopic steady-state = $+45\text{\textperthousand}$, 8: riverine $\delta^{34}\text{S}$ value = $+5\text{\textperthousand}$). (a) Sulfate input is slightly greater than sulfate output, and both are unchanged for the duration of the model. (b) The mass of the sulfate reservoir increases linearly with model time. (c) $\Delta^{17}\text{O}_s$ responds to a step function change in $\Delta^{17}\text{O}_W$, reaching a steady state value equal to $\Delta^{17}\text{O}_W$. (d) $\delta^{34}\text{S}_s$ responds to the fractionation associated with microbial sulfur cycling (${}^{34}\varepsilon$), reaching a steady state value modulated by the magnitude of f_{py} . (For interpretation of the references to color in this figure legend, the reader is referred to the web version of this article.)

total amount of sulfate in the post-Marinoan ocean in this model (Peng et al., 2011). This characteristic contrasts with evidence for growth of the marine sulfate reservoir during the Ediacaran period (Halverson and Hurtgen, 2007; Sahoo et al., 2012). In addition, the model's suggestion of an apparent oxidative inversion, where modern levels of sulfide re-oxidation in the ocean are sustained in the face of limited oxidative weathering of continental sulfide minerals, runs counter to evidence for the immediate resumption of oxygenic primary productivity in the post-glacial photic zone (Kunzmann et al., 2013) in a post-Marinoan ocean that was anoxic overall (Johnston et al., 2013). It is further difficult to envision how the oxidizing capacity in the ocean is kept separate from the troposphere. These challenges led us to develop a new quantitative interpretation of the unique isotopic trends preserved in post-Marinoan seafloor barites.

4.2. Isotopic evolution of the post-Marinoan sulfur cycle

The variability in $\delta^{34}\text{S}$ observed within global cap carbonate sequences requires either a diminished global sulfate reservoir, or local processes that act simultaneously on nearly every paleo-continent producing isotopic trends of the same magnitude and direction (Hurtgen et al., 2006). The oxygen and sulfur isotopic signatures preserved within the Ravensthorpe barite are similar to those in post-Marinoan barite preserved on other paleo-continents as well as isotopic signatures preserved within cap carbonates in Australia (Shields et al., 2007; Bao et al., 2008, 2012; Peng et al., 2011). As a result, this consistency points toward a common solution, and one that operates on a global-scale.

We assert that the basic processes of the marine sulfur cycle (MSR, pyrite burial, and sulfate input from continental weathering)

are able to reproduce the collective isotopic observations when operating under realistic conditions for the post-Marinoan oceans. First, the anomalous oxygen isotope composition in the barites resulted from the specific atmospheric and biospheric state that evolved during the Marinoan glaciation (Bao et al., 2008), and was carried to the ocean via the oxidative weathering of continental sulfides (Bao et al., 2009). Enhanced oxidative weathering was likely behind the inferred increase in the size of the marine sulfate reservoir as the Ediacaran period progressed, requiring the flux of sulfate from the continents to outpace sulfate removal through pyrite burial (Halverson and Hurtgen, 2007; Sahoo et al., 2012). In order to test this scenario, we constructed a dynamic 1-box model of the marine sulfur cycle (cf. Halverson and Hurtgen, 2007). The model is described in Equations (5)–(7), where all calculations were performed using delta notation, and key model inputs and outputs are conceptually summarized in Fig. 3 and detailed in Table 2.

$$dM_s/dt = F_w - F_w \times f_{py} \quad (5)$$

$$d(M_s \times \delta^{34}\text{S}_s)/dt = F_w \times \delta^{34}\text{S}_w - f_{py} \times F_w \times (\delta^{34}\text{S}_s + {}^{34}\varepsilon) \quad (6)$$

$$d(M_s \times \Delta^{17}\text{O}_s)/dt = F_w \times \Delta^{17}\text{O}_w - f_{py} \times F_w \times (\Delta^{17}\text{O}_s) \quad (7)$$

The initial isotopic composition of the marine sulfate reservoir is set at $\Delta^{17}\text{O}_{s0} = -0.1\text{\textperthousand}$ (Bao et al., 2012) and $\delta^{34}\text{S}_{s0} = +15\text{\textperthousand}$ (Halverson and Hurtgen, 2007). The model has two free parameters: (1) the fraction (f_{py}) of the flux of sulfate coming into the system by weathering (F_w) that leaves the system via pyrite burial ($F_{\text{pyrite burial}}$) where $f_{py} = F_{\text{pyrite burial}}/F_w$; and (2) the fractionation associated with MSR that is imparted to the pyrite leaving the system [${}^{34}\varepsilon = ({}^{34}\alpha - 1) \times 1000 \approx \delta^{34}\text{S}_{\text{py}} - \delta^{34}\text{S}_s$, where ${}^{34}\alpha = ([{}^{34}\text{S}/{}^{32}\text{S}]_{\text{py}}/[{}^{34}\text{S}/{}^{32}\text{S}]_s)$]. Re-oxidation of sulfide to sulfate is not considered directly in this model (Figs. 3a, 3b), although the

Table 2

Summary of reference model input parameters with end-member possibilities considered in model sensitivity tests.

Parameter	Description	Reference model value	Sensitivity tests
M_{S0}	Initial marine sulfate concentration	$3 \cdot 10^{16}$ mol	–
F_w	Weathering flux of sulfate	$3 \cdot 10^{12}$ mol yr ⁻¹	$\approx 3 \cdot 10^{11}$ to $3 \cdot 10^{13}$ mol yr ⁻¹
$\Delta^{17}\text{O}_{w0}$	$\Delta^{17}\text{O}$ value of initial sulfate weathering flux	-4.2‰	–
$\Delta^{17}\text{O}_{s0}$	$\Delta^{17}\text{O}$ value of initial marine sulfate reservoir	-0.1‰	–
$\Delta^{17}\text{O}_{\min}$	Minimum $\Delta^{17}\text{O}$ value reached by marine sulfate	-1.0‰	–
$\Delta^{17}\text{O}_{ws}$	$\Delta^{17}\text{O}$ value of sulfate weathering flux once $\Delta^{17}\text{O}_{\min}$ (-1.0‰) is achieved	-0.1‰	–
$\Delta^{17}\text{O}_s$	Calculated $\Delta^{17}\text{O}$ of marine sulfate	–	–
$\delta^{34}\text{S}_w$	$\delta^{34}\text{S}$ value of sulfate weathering flux	+5.0‰	–
$\delta^{34}\text{S}_{s0}$	$\delta^{34}\text{S}$ value of initial sulfate reservoir	+15.0‰	–
$\delta^{34}\text{S}_{py}$	$\delta^{34}\text{S}$ of pyrite produced from MSC	–	–
$\delta^{34}\text{S}_s$	Calculated $\delta^{34}\text{S}$ of marine sulfate	–	–
$^{34}\varepsilon$	≈ the difference in $\delta^{34}\text{S}$ values of sulfate and sulfide	-42‰	-37‰ to -47‰
f_{py}	Fraction of sulfate leaving the system via pyrite burial	0.95	0.85–1.05
τ	Marine sulfate residence time	10^4 yr	$>10^3$, $<10^6$ yr
λ	Mass law exponent for MSC	–	0.505–0.520

potential sulfur isotope consequences of re-oxidation are explored later.

We forced the model with an initial pulse of ^{17}O -depleted sulfate with $\Delta^{17}\text{O}_{w0} = -4.2\text{\textperthousand}$, and $\delta^{34}\text{S}_w = +5\text{\textperthousand}$, which represents one plausible observationally constrained estimate of the isotopic composition of weathering-derived sulfate following the Marinoan glaciation (Bao et al., 2009; Halverson and Hurtgen, 2007; Figs. 3c, 3d). The assumption of a constant isotopic composition for weathering-derived sulfate is a simplification, and the isotopic composition of atmospheric O_2 is likely to be globally homogeneous on the timescales considered here. However strict transfer of this isotopic homogeneity to sulfate derived from oxidation of terrestrial sulfides is unlikely. The minimum $\Delta^{17}\text{O}$ value observed in the barite dataset ($\Delta^{17}\text{O}_{\min} = -1.0\text{\textperthousand}$) is interpreted to reflect the minimum $\Delta^{17}\text{O}$ value reached by the marine sulfate reservoir, and constrains the duration of the initial pulse of ^{17}O -depleted sulfate carried by continental run-off as a result (Fig. 3c). This timing also constrains the period over which the specific $p\text{O}_2$ and $p\text{CO}_2$ necessary to generate the prescribed $\Delta^{17}\text{O}$ were present. We assume that the $\Delta^{17}\text{O}$ values carried by F_w decreased the $\Delta^{17}\text{O}$ of marine sulfate from -0.1‰ to a minimum value of -1‰, and upon reaching this value barite deposition initiated. This assumption enables a timing estimate of the duration of the initial ^{17}O depleted pulse from continental run-off, and also provides a maximum duration for the deposition of the underlying cap dolostone. The shift from isotopically anomalous riverine $\Delta^{17}\text{O}$ values to isotopically normal values characterized by $\Delta^{17}\text{O}_{w0} = -0.1\text{\textperthousand}$ is taken as a step function in the model (Fig. 3c). Although the transition from a high $p\text{CO}_2$ syn-glacial atmosphere with limited primary production to a more characteristic Ediacaran environment with lower $p\text{CO}_2$ values and renewed primary production is unlikely to

be instantaneous, it appears to be rapid (Sansjofer et al., 2011; Bao et al., 2012; Killingsworth et al., 2013; Kunzmann et al., 2013).

The forcing used here captures the first-order isotopic consequences of this transition without adding unconstrained temporal complexity. The progression of marine sulfate isotope compositions toward steady-state values of $\Delta^{17}\text{O}_s = -0.1\text{\textperthousand}$ tracks dilution with isotopically normal riverine sulfate (Fig. 3c), while the $\delta^{34}\text{S}$ value approaching 45‰ reflects fractionation associated with sulfate removal through MSR, modified by the relative fraction of pyrite burial compared to weathering (Fig. 3d). These isotopic endpoints are fixed by our measurements from northwest Canada (Table 1), which are corroborated by previous studies in South China and Mauritania (Bao et al., 2008; Peng et al., 2011; Killingsworth et al., 2013). The evolution of the model is set by the passage of sulfate turnover times ($\tau = M_{S0}/F_w$; the ratio of the initial mass of marine sulfate to the influx of sulfate from continental weathering).

In Fig. 4 we present a sensitivity analysis of the model to changing parameters ($^{34}\varepsilon$, f_{py}). The reference model used $^{34}\varepsilon = -42\text{\textperthousand}$ and $f_{py} = 0.95$ to reproduce the $\Delta^{17}\text{O}$ and $\delta^{34}\text{S}$ evolution of the B1–B3 barite layers (Fig. 4). Although the reference $^{34}\varepsilon$ value is near the upper limit of measured $\delta^{34}\text{S}$ differences between pyrite and carbonate associated sulfate in Marinoan cap dolostones (Hurtgen et al., 2005, 2006), it is within the range of theoretical predictions (Wing and Halevy, 2014) and experimental determinations (Sim et al., 2011; Leavitt et al., 2013; Bradley et al., 2016) of MSC at low sulfate concentrations. The reference model generated a close isotopic match in model time for each of the barite horizons, thus we consider it a plausible set of conditions to explain coherent stratigraphic variations observed here. We tested each model run for fidelity with the rock record by verifying that the model output $\Delta^{17}\text{O}$ values corresponding with measured B1 (-0.66), B2 (-0.39), and B3 (-0.12) were produced within the same model time period as the equivalent measured $\delta^{34}\text{S}$ values for B1 (29.1 ± 4.3), B2 (39.5 ± 4.4) and B3 (44.4 ± 2.5). Dotted circles in Fig. 4 indicate compatibility among model and data. Three model cases (Figs. 4a, 4e, and 4i) were found to be compatible with all measured data requiring a value for f_{py} near 1, and a value for $^{34}\varepsilon$ near -40‰. Independently increasing the reference model $^{34}\varepsilon$ to -37‰ or lowering $^{34}\varepsilon$ to -47‰ without changing f_{py} resulted in a poor model fit (Fig. 4d, 4f). A decreasing sulfate reservoir size with time was investigated by increasing f_{py} to 1.05, thereby requiring consumption of the standing pool of sulfate. Increasing f_{py} above 1 did not result in compatible solutions with $^{34}\varepsilon$ set at -42‰ or -47‰ (Figs. 4b, 4c), but was compatible with $^{34}\varepsilon = -37\text{\textperthousand}$. Decreasing f_{py} to 0.85 resulted in a model fit with less compatibility as $^{34}\varepsilon$ values increased (Figs. 4g, 4h). Thus, there is a narrow range of parameters that can be used in this model to reproduce the isotopic measurements in the Ravensthorpe formation, resulting in a narrow set of non-unique solutions that are consistent with current understanding of MSC. Our model suggests that f_{py} needs to be close to, but not greater than 1 and $^{34}\varepsilon$ values are approximately -40‰, which is typical for $^{34}\varepsilon$ values in marine sediments (Leavitt et al., 2013).

These results highlight three important features of the post-Marinoan marine sulfur cycle. First, the marine sulfate reservoir was predisposed to isotopic modification in the immediate aftermath of the Marinoan glaciation. Second, these isotopic changes occurred over approximately four to five turnover times of the marine sulfate reservoir ($\tau = 4–5$). Third, since the deposition of the cap dolostones occurred prior to the barite layers, the duration of the initial ^{17}O depleted weathering pulse suggests that the cap dolostones were deposited in less than one turnover time of the marine sulfate reservoir ($\tau = 0.3$).

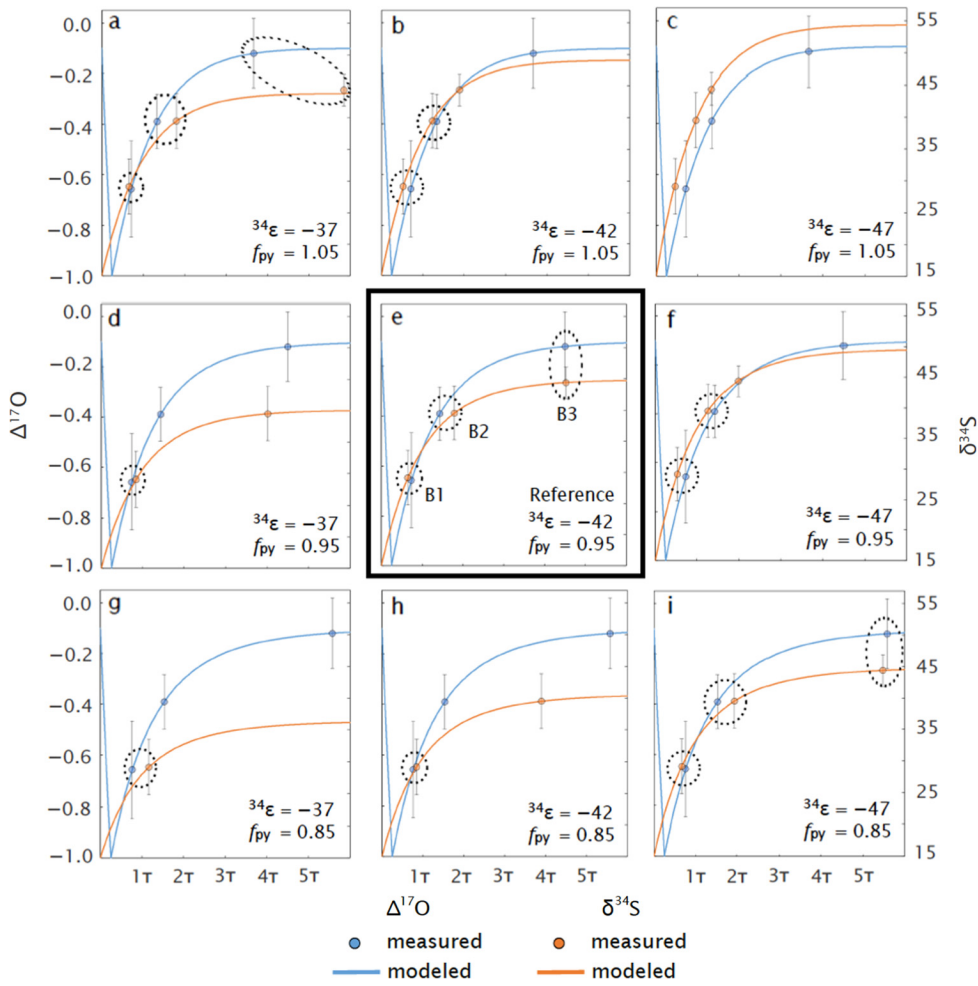


Fig. 4. Model sensitivity to changes in isotope fractionation between sulfate and sulfide ($^{34}\epsilon$) and pyrite burial flux (f_{py}) relative to weathering flux (F_w). Data points represent the mean isotopic compositions of barite layers B1–B3. Error bars represent 2σ on the mean of the measurements from each respective layer. Dotted circles indicate agreement in model time between the mean values $\pm 2\sigma$ for $\Delta^{17}\text{O}$ and $\delta^{34}\text{S}$.

4.3. $\Delta^{33}\text{S}-\delta^{34}\text{S}$ patterns in post-Marinoan seafloor barite

In contrast to previous models of the post-Marinoan sulfur cycle (Peng et al., 2011), the reference presented here explains the data set without contributions from sulfide re-oxidation. Measured multiple sulfur isotope values provide an independent test of this prediction (Fig. 2b). Sulfur-based microbial metabolisms can lead to small $\delta^{33}\text{S}-\delta^{34}\text{S}$ deviations from the reference mass law defined by $^{33}\lambda = 0.515$ through their impact on sulfur isotope fractionation factors. The exponential relationship between fractionation factors of different isotope pairs is typically expressed through λ values, where, for example, $^{33}\alpha = ^{34}\alpha \cdot ^{33}\lambda$. Through an equation like (7) for $\delta^{33}\text{S}$, we incorporated fractionation of $^{33}\text{S}-^{32}\text{S}$ associated with MSC and pyrite burial in the reference model ($^{34}\epsilon = -42\%$; $f_{\text{py}} = 0.95$), and predicted the $\Delta^{33}\text{S}-\delta^{34}\text{S}$ patterns that result from different values of $^{33}\lambda$. Starting from an initial $\delta^{34}\text{S}_{\text{SO}} = +15\text{\textperthousand}$ and $\Delta^{33}\text{S}_{\text{SO}} = -0.05$ (Scott et al., 2014), the $\Delta^{33}\text{S}-\delta^{34}\text{S}$ trajectory from the Ravensthrat barite is inconsistent with $^{33}\lambda$ values associated with re-oxidative sulfur cycling via microbial disproportionation of elemental sulfur or sulfite (Fig. 2b; $^{33}\lambda = 0.515-0.520$; Johnston et al., 2005; Pellerin et al., 2015a), but falls along the lower limit of predictions based on laboratory and theoretical studies of $^{33}\lambda$ values generated by MSR only (Fig. 2b; $^{33}\lambda = 0.505-0.515$) (Farquhar et al., 2003; Johnston et al., 2005; Wu et al., 2010; Leavitt et al., 2013; Wing and Halevy, 2014; Pellerin et al., 2015b).

Our inference that the $\Delta^{33}\text{S}-\delta^{34}\text{S}$ patterns reflect primarily MSR is reinforced by the $\delta^{18}\text{O}$ values of the Ravensthrat barite. Although they were not modeled due to a lack of constraints on the $\delta^{18}\text{O}$ of the post-glacial hydrosphere, similar $\delta^{18}\text{O}$ values, along with elevated $\delta^{34}\text{S}$ values, are characteristic of sulfate undergoing active MSR in modern environments (Antler et al., 2013, 2015). In general, the additional isotopic evidence presented here is further support for a post-Marinoan global marine sulfate reservoir that is driven by post-glacial resumption of continental weathering, MSR, and pyrite burial.

4.4. Sulfate source to post-Marinoan seafloor barite

In Fig. 5, we plot the results of the reference model of marine sulfate evolution in $\delta^{34}\text{S}$ and $\Delta^{17}\text{O}$ space, overlain by the Ravensthrat barite data. The ability of the model to reproduce the measured patterns implies that the sulfate source to the seafloor barite in northwest Canada could be a global seawater reservoir. As a consequence, the modeled seawater sulfate values could plausibly be compositional end-members during barite deposition on other paleo-continents.

Previously published $\delta^{34}\text{S}$ and $\Delta^{17}\text{O}$ values from well preserved barites with little to no diagenetic overprinting from South China (Fig. 5; Peng et al., 2011) scatter away from modeled oceanic values and toward higher $\Delta^{17}\text{O}$ and lower $\delta^{34}\text{S}$, thus requiring a second source of sulfate. One possible explanation is that the South China succession may represent a system with a stronger riverine

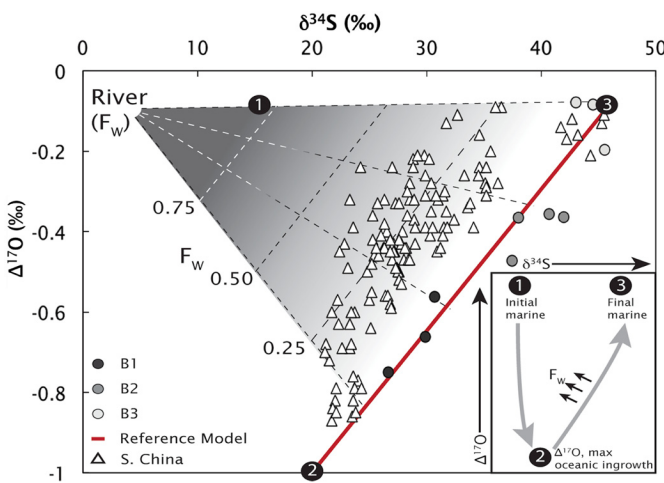


Fig. 5. Cross-plot of $\Delta^{17}\text{O}$ and $\delta^{34}\text{S}$ values from the reference model (${}^{34}\varepsilon = -42\text{‰}$, $f_{\text{py}} = 0.95$) from the Ravensthorpe Formation barites from northwest Canada (B1, B2 and B3), and from the Doushantuo Formation barites from South China (Peng et al., 2011). Mixing between the evolving marine sulfate reservoir (model) and post-glacial riverine sulfate creates a mixing surface by which contributions from each end-member can be determined for the South China data set. Marine sulfate isotopic composition evolves from an initial composition (1) to the most extreme ^{17}O values where F_w steps from $\Delta^{17}\text{O} = -4.2\text{‰}$ to $\Delta^{17}\text{O} = -0.1\text{‰}$ (2), and finally marine isotopic values captured in barites evolve along the red line to a final isotopic composition (3). Please refer to Fig. 2 for analytical uncertainty. (For interpretation of the references to color in this figure legend, the reader is referred to the web version of this article.)

influence than that of northwest Canada. This is evidenced through barite deposition occurring over a larger stratigraphic interval in South China in shallower carbonate facies that would plausibly have faster accumulation rates than the northwest Canada samples (Peng et al., 2011). We suggest that isotopically normal riverine sulfate (with a $\Delta^{17}\text{O}$ value of -0.1‰ after the initial pulse of ^{17}O depleted sulfate) is mixed with an open ocean sulfate pool (with an evolving $\Delta^{17}\text{O}$) during the time of barite deposition in South China, creating a spectrum of compositions between these end-members (Fig. 5). This mixing relationship suggests that the South China barite layers record up to 50% dilution of marine sulfate via sulfate supplied by rivers. Together with our model solution, this interpretation of the South China dataset provides a globally consistent framework for the isotopic evolution of these and other post-Marinoan barite deposits.

4.5. Calibrating the size of the post-Marinoan sulfate reservoir

The reference model constrains the residence time of marine sulfate during the immediate aftermath of the Marinoan glaciation, if the timeframes of cap dolostone and barite accumulation can be estimated. There is only a single estimate of the time interval represented by post-Marinoan seafloor barite horizons: $2.1 \pm 7.8 \times 10^5$ yr estimated by correlating $\delta^{13}\text{C}$ patterns from the Marinoan sections in South China (Killingsworth et al., 2013). In contrast, there is a wide range of estimates for the time interval represented by the cap dolostones, from $\approx 10^3$ yr (oceanographic models; Hyde et al., 2000), $\approx 10^4$ yr (modeling of sea level changes; Creveling and Mitrovica, 2014), $\approx 10^5$ yr (paleomagnetic reversal frequencies; Trindade et al., 2003), to $\approx 10^6$ yr (Ca and Mg isotope modeling; Kasemann et al., 2014). If the duration of barite accumulation was 2×10^5 yr (Killingsworth et al., 2013), then the modeling presented here suggests that $\Delta^{17}\text{O}$ ingrowth into the marine sulfate reservoir and, by inference, the deposition of the cap dolostone occurred on the order of $\approx 10^4$ yr. This timescale is consistent with a recent estimate of the lifetime of a post-glacial meltwater plume in the post-Marinoan ocean (Liu et al., 2014). Under this timescale, the

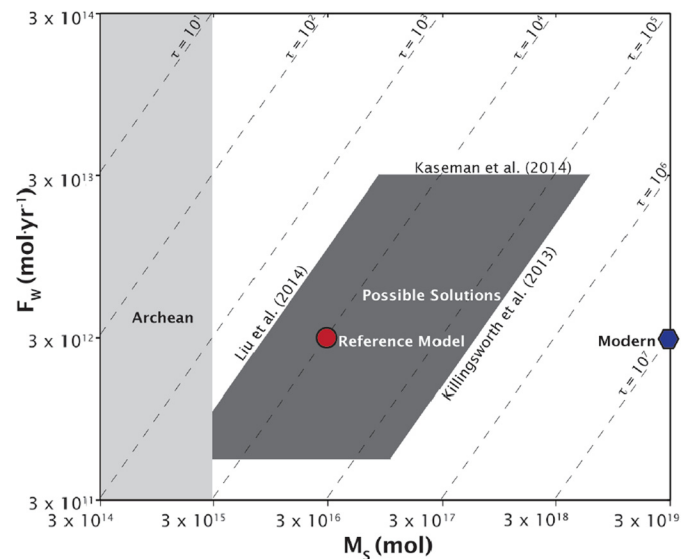


Fig. 6. Summary of estimated upper and lower potential limits on turnover times of the marine sulfate reservoir (M_s/F_w) and F_w (see Jamieson et al., 2013; Killingsworth et al., 2013; Kasemann et al., 2014; Liu et al., 2014). Gridlines represent varying residence time values (τ) in years. Model solutions compatible with the Ravensthorpe $\Delta^{17}\text{O}$ and $\delta^{34}\text{S}$ data are represented in the dark grey box, which deviates from the τ isolines in the lower left to disregard solutions that have a M_s below estimated Archean sulfate concentrations (shown as a light grey box). The reference model solution is represented by the red circle where $M_s/F_w = 10^4$ yr. The modern sulfur cycle is represented as a blue hexagon, and plots well outside of the possible post-Marinoan solutions. (For interpretation of the references to color in this figure legend, the reader is referred to the web version of this article.)

reference model suggests that the residence time of sulfate in the post-Marinoan ocean was $\approx 4\text{--}5 \times 10^4$ yr (Fig. 4).

We suggest a modern weathering flux is a plausible estimate of post-glacial sulfate supply to the marine reservoir. Given the absence of mass-independent sulfur isotope fractionation in the barites, it is unlikely $p\text{O}_2$ levels dropped to sufficiently low values during the glaciation to hinder pyrite oxidation (Reinhard et al., 2013), while a vigorous post-glacial hydrologic cycle (Kasemann et al., 2014) would likely outpace modern riverine input. With a modern flux of sulfate from continental weathering, a residence time of $\approx 10^4$ yr implies a small marine sulfate reservoir at the end of the Marinoan glacial interval (Fig. 6; $\approx 0.1\%$ of modern marine sulfate). For a barite accumulation interval of 10^6 yr (the maximum allowed by chronologic uncertainties; Killingsworth et al., 2013) and a larger sulfate supply from enhanced post-Marinoan continental weathering ($10\times$ modern; Kasemann et al., 2014), an upper limit to the post-Marinoan sulfate pool approaching 10% modern is implied (Fig. 6). These values bracket published estimates of marine sulfate concentrations at the start of the Ediacaran period (1% of modern; Halverson and Hurtgen, 2007). Low but increasing sulfate concentrations appear to have been maintained throughout the deposition of the seafloor barite, as the coupled oxygen and sulfur isotope variations require that much, but not all, of the sulfate coming into the post-Marinoan ocean was reduced to sulfide and sequestered as pyrite.

5. Conclusions

In this study we have extended the previously reported $\Delta^{17}\text{O}$ anomalies in post-Marinoan marine barite precipitates to a new paleo-continent, highlighting the global nature of this geochemical horizon. By pairing these results with coeval multiple sulfur isotope analyses we provide new insights into the post-Marinoan sulfur cycle and climate. First we demonstrate the dynamic nature of the sulfur cycle, where the $\Delta^{17}\text{O}$ anomaly can be imparted

and subsequently eliminated in four to five turnovers of the marine sulfate reservoir. Second, our results suggest that this can be achieved through oxidative weathering coupled to microbial sulfate reduction and pyrite burial, without much contribution from re-oxidative fluxes. Further, and a target for subsequent work, is the implication that the post-Marinoan atmosphere (here involving CO₂, O₂ and gross primary production) was evolving in a fashion whereby the magnitude of the tropospheric Δ¹⁷O anomaly in O₂ crashed as the ocean-atmosphere recovered following the glaciation. Third, we show that the initial post-Marinoan sulfate reservoir was smaller than at other times in the Ediacaran, possibly 0.1% modern with an upper limit of 10% modern. Finally our results appear to be most consistent with recent timing estimates of cap carbonate deposition on the order of ~10⁴ yr, reminiscent of timescales that have come to characterize typical glacial-interglacial cycles. Together these findings highlight that the post-Marinoan sulfur cycle was not different from the modern with respect to important processes, however, it was likely unfamiliar with respect to magnitudes of sources and sinks.

Acknowledgements

We give special thanks to Dr. Huiming Bao for enlightening discussions about triple oxygen isotopes and for access to the OA-SIC laboratory at Louisiana State University. We would also like to thank two anonymous reviewers and Pierre Cartigny for constructive reviews and AE Gideon Henderson for editorial guidance that greatly improved this manuscript. The National Science and Engineering Research Council of Canada supported this work through a Canadian Astrobiology Training Program PhD Fellowship to PWC and NSERC CREATE and Discovery Grants RGPIN-2014-06626 to BAW. Fieldwork was supported by NSF Grant EAR-0417422 (PFH). The Stable Isotope Laboratory at McGill is supported by the FQRNT through the GEOTOP research center. Cowie and Johnston were funded through the MIT-Harvard node of the NASA NAI as well as a NSF CAREER award to DTJ.

References

- Antler, G., Turchyn, A.V., Rennie, V., Herut, B., Sivan, O., 2013. Coupled sulfur and oxygen isotope insight into bacterial sulfate reduction in the natural environment. *Geochim. Cosmochim. Acta* 118, 98–117.
- Antler, G., Turchyn, A.V., Herut, B., Sivan, O., 2015. A unique isotopic fingerprint of sulfate-driven anaerobic oxidation of methane. *Geology*, G36688-1.
- Arnaud, E., Halverson, G.P., Shields-Zhou, G. (Eds.), 2011. The Geological Record of Neoproterozoic Glaciations. Geological Society of London.
- Balci, N., Shanks III, W.C., Mayer, B., Mandernack, K.W., 2007. Oxygen and sulfur isotope systematics of sulfate produced by bacterial and abiotic oxidation of pyrite. *Geochim. Cosmochim. Acta* 71 (15), 3796–3811.
- Bao, H., 2006. Purifying barite for oxygen isotope measurement by dissolution and reprecipitation in a chelating solution. *Anal. Chem.* 78 (1), 304–309.
- Bao, H., Thiemens, M.H., 2000. Generation of O₂ from BaSO₄ using a CO₂-laser fluorination system for simultaneous analysis of δ¹⁸O and δ¹⁷O. *Anal. Chem.* 72 (17), 4029–4032.
- Bao, H., Lyons, J.R., Zhou, C., 2008. Triple oxygen isotope evidence for elevated CO₂ levels after a Neoproterozoic glaciation. *Nature* 453 (7194), 504–506.
- Bao, H., Fairchild, I.J., Wynn, P.M., Spötl, C., 2009. Stretching the envelope of past surface environments: Neoproterozoic glacial lakes from Svalbard. *Science* 323 (5910), 119–122.
- Bao, H., Chen, Z.Q., Zhou, C., 2012. An Δ¹⁷O record of late Neoproterozoic glaciation in the Kimberley region, Western Australia. *Precambrian Res.* 216, 152–161.
- Bradley, A.S., Leavitt, W.D., Schmidt, M., Knoll, A.H., Gireuis, P.R., Johnston, D.T., 2016. Patterns of sulfur isotope fractionation during Microbial Sulfate Reduction. *Geobiology*. <http://dx.doi.org/10.1111/gbi.12149>.
- Butchart, N., Scaife, A.A., Bourqui, M., De Grandpré, J., Hare, S.H.E., Kettleborough, J., Langenatz, U., Manzini, E., Sassi, F., Shibata, K., Shindell, D., Signond, M., 2006. Simulations of anthropogenic change in the strength of the Brewer-Dobson circulation. *Clim. Dyn.* 27 (7–8), 727–741.
- Canfield, D.E., Thamdrup, B., 1994. The production of ³⁴S-depleted sulfide during bacterial disproportionation of elemental sulfur. *Science* 266 (5193), 1973–1975.
- Canfield, D.E., Teske, A., 1996. Late Proterozoic rise in atmospheric oxygen concentration inferred from phylogenetic and sulphur-isotope studies. *Nature* 382 (6587), 127–132.
- Canfield, D.E., Raiswell, R., Westrich, J.T., Reaves, C.M., Berner, R.A., 1986. The use of chromium reduction in the analysis of reduced inorganic sulfur in sediments and shales. *Chem. Geol.* 54 (1), 149–155.
- Cao, X., Bao, H., 2013. Dynamic model constraints on oxygen-17 depletion in atmospheric O₂ after a snowball Earth. *Proc. Natl. Acad. Sci.* 110 (36), 14546–14550.
- Creveling, J.R., Mitrovica, J.X., 2014. The sea-level fingerprint of a Snowball Earth deglaciation. *Earth Planet. Sci. Lett.* 399, 74–85.
- Farquhar, J., Johnston, D.T., Wing, B.A., Habicht, K.S., Canfield, D.E., Airieau, S., Thiemens, M.H., 2003. Multiple sulphur isotopic interpretations of biosynthetic pathways: implications for biological signatures in the sulphur isotope record. *Geobiology* 1 (1), 27–36.
- Gomes, M.L., Hurtgen, M.T., 2015. Sulfur isotope fractionation in modern euxinic systems: implications for paleoenvironmental reconstructions of paired sulfate-sulfide isotope records. *Geochim. Cosmochim. Acta* 157, 39–55.
- Halverson, G.P., Hurtgen, M.T., 2007. Ediacaran growth of the marine sulfate reservoir. *Earth Planet. Sci. Lett.* 263 (1), 32–44.
- Hoffman, P.F., Halverson, G.P., 2011. Neoproterozoic glacial record in the Mackenzie Mountains, northern Canadian Cordillera. *Mem. Geol. Soc. Lond.* 36 (1), 397–412.
- Hoffman, P.F., Kaufman, A.J., Halverson, G.P., Schrag, D.P., 1998. A Neoproterozoic snowball earth. *Science* 281 (5381), 1342–1346.
- Hoffman, P.F., Macdonald, F.A., Halverson, G.P., 2011. Chemical sediments associated with Neoproterozoic glaciation: iron formation, cap carbonate, barite and phosphorite. *Mem. Geol. Soc. Lond.* 36 (1), 67–80.
- Hurtgen, M.T., Arthur, M.A., Halverson, G.P., 2005. Neoproterozoic sulfur isotopes, the evolution of microbial sulfur species, and the burial efficiency of sulfide as sedimentary pyrite. *Geology* 33 (1), 41–44.
- Hurtgen, M.T., Halverson, G.P., Arthur, M.A., Hoffman, P.F., 2006. Sulfur cycling in the aftermath of a 635-Ma snowball glaciation: evidence for a syn-glacial sulfidic deep ocean. *Earth Planet. Sci. Lett.* 245 (3), 551–570.
- Hyde, W.T., Crowley, T.J., Baum, S.K., Peltier, W.R., 2000. Neoproterozoic ‘snowball Earth’ simulations with a coupled climate/ice-sheet model. *Nature* 405 (6785), 425–429.
- Jamieson, J.W., Wing, B.A., Farquhar, J., Hannington, M.D., 2013. Neoarchean seawater sulphate concentrations from sulphur isotopes in massive sulphide ore. *Nat. Geosci.* 6 (1), 61–64.
- Jiang, G., Kennedy, M.J., Christie-Blick, N., Wu, H., Zhang, S., 2006. Stratigraphy, sedimentary structures, and textures of the late Neoproterozoic Doushantuo cap carbonate in South China. *J. Sediment. Res.* 76 (7), 978–995.
- Jørgensen, B.B., 1990. A thiosulfate shunt in the sulfur cycle of marine sediments. *Science* 249 (4965), 152–154.
- Johnston, D.T., Wing, B.A., Farquhar, J., Kaufman, A.J., Strauss, H., Lyons, T.W., Kah, L., Canfield, D.E., 2005. Active microbial sulfur disproportionation in the Mesoproterozoic. *Science* 310 (5753), 1477–1479.
- Johnston, D.T., Poultney, S.W., Tosca, N.J., O'Brien, T., Halverson, G.P., Schrag, D.P., Macdonald, F.A., 2013. Searching for an oxygenation event in the fossiliferous Ediacaran of northwestern Canada. *Chem. Geol.* 362, 273–286.
- Johnston, D.T., Gill, B.C., Masterson, A., Beirne, E., Casciotti, K.L., Knapp, A.N., Berelson, W., 2014. Placing an upper limit on cryptic marine sulphur cycling. *Nature*.
- Kasemann, S.A., Pogge von Strandmann, P.A., Prave, A.R., Fallick, A.E., Elliott, T., Hoffmann, K.H., 2014. Continental weathering following a Cryogenian glaciation: evidence from calcium and magnesium isotopes. *Earth Planet. Sci. Lett.* 396, 66–77.
- Kennedy, M.J., 1996. Stratigraphy, sedimentology, and isotopic geochemistry of Australian Neoproterozoic postglacial cap dolostones: deglaciation, δ¹³C excursions, and carbonate precipitation. *J. Sediment. Res.* 66 (6).
- Killingsworth, B.A., Hayles, J.A., Zhou, C., Bao, H., 2013. Sedimentary constraints on the duration of the Marinoan Oxygen-17 Depletion (MOSD) event. *Proc. Natl. Acad. Sci.* 110 (44), 17686–17690.
- Kohl, I., Bao, H., 2011. Triple-oxygen-isotope determination of molecular oxygen incorporation in sulfate produced during abiotic pyrite oxidation (pH = 2–11). *Geochim. Cosmochim. Acta* 75 (7), 1785–1798.
- Kunzmann, M., Halverson, G.P., Sossi, P.A., Raub, T.D., Payne, J.L., Kirby, J., 2013. Zn isotope evidence for immediate resumption of primary productivity after snowball Earth. *Geology* 41 (1), 27–30.
- Leavitt, W.D., Halevy, I., Bradley, A.S., Johnston, D.T., 2013. Influence of sulfate reduction rates on the Phanerozoic sulfur isotope record. *Proc. Natl. Acad. Sci.* 110 (28), 11244–11249.
- Liu, C., Wang, Z., Raub, T.D., Macdonald, F.A., Evans, D.A., 2014. Neoproterozoic cap-dolostone deposition in stratified glacial meltwater plume. *Earth Planet. Sci. Lett.* 404, 22–32.
- Luz, B., Barkan, E., Bender, M.L., Thiemens, M.H., Boering, K.A., 1999. Triple-isotope composition of atmospheric oxygen as a tracer of biosphere productivity. *Nature* 400 (6744), 547–550.
- Macdonald, F.A., Strauss, J.V., Sperling, E.A., Halverson, G.P., Narbonne, G.M., Johnston, D.T., Kunzmann, M., Schrag, D.P., Higgins, J.A., 2013. The stratigraphic relationship between the Shuram carbon isotope excursion, the oxygenation of Neoproterozoic oceans, and the first appearance of the Ediacara biota and bilaterian trace fossils in northwestern Canada. *Chem. Geol.* 362, 250–272.

- Pellerin, A., Bui, T.H., Rough, M., Mucci, A., Canfield, D.E., Wing, B.A., 2015a. Mass-dependent sulfur isotope fractionation during reoxidative sulfur cycling: a case study from Mangrove Lake, Bermuda. *Geochim. Cosmochim. Acta* 149, 152–164.
- Pellerin, A., Anderson-Trocmé, L., Whyte, L.G., Zane, G.M., Wall, J.D., Wing, B.A., 2015b. Sulfur isotope fractionation during the evolutionary adaptation of a sulfate-reducing bacterium. *Appl. Environ. Microbiol.* 81 (8), 2676–2689.
- Peng, Y., Bao, H., Zhou, C., Yuan, X., 2011. $\Delta^{17}\text{O}$ -depleted barite from two Marinoan cap dolostone sections, South China. *Earth Planet. Sci. Lett.* 305 (1), 21–31.
- Reinhard, C.T., Lalonde, S.V., Lyons, T.W., 2013. Oxidative sulfide dissolution on the early Earth. *Chem. Geol.* 362, 44–55.
- Sahoo, S.K., Planavsky, N.J., Kendall, B., Wang, X., Shi, X., Scott, C., Anbar, A., Lyons, T.W., Jiang, G., 2012. Ocean oxygenation in the wake of the Marinoan glaciation. *Nature* 489 (7417), 546–549.
- Sansjofre, P., Ader, M., Trindade, R.I.F., Elie, M., Lyons, J., Cartigny, P., Nogueira, A.C.R., 2011. A carbon isotope challenge to the snowball Earth. *Nature* 478 (7367), 93–96.
- Scott, C., Wing, B.A., Bekker, A., Planavsky, N.J., Medvedev, P., Bates, S.M., Yun, M., Lyons, T.W., 2014. Pyrite multiple-sulfur isotope evidence for rapid expansion and contraction of the early Paleoproterozoic seawater sulfate reservoir. *Earth Planet. Sci. Lett.* 389, 95–104.
- Shields, G.A., Deynoux, M., Strauss, H., Paquet, H., Nahon, D., 2007. Barite-bearing cap dolostones of the Taoudéni Basin, northwest Africa: sedimentary and isotopic evidence for methane seepage after a Neoproterozoic glaciation. *Precambrian Res.* 153 (3), 209–235.
- Sim, M.S., Bosak, T., Ono, S., 2011. Large sulfur isotope fractionation does not require disproportionation. *Science* 333 (6038), 74–77.
- Thiemens, M.H., Heidenreich, J.E., 1983. The mass-independent fractionation of oxygen: a novel isotope effect and its possible cosmochemical implications. *Science* 219 (4588), 1073–1075.
- Thode, H.G., Monster, Jan, Dunford, H.B., 1961. Sulphur isotope geochemistry. *Geochim. Cosmochim. Acta* 25 (3), 159–174.
- Torres, M.E., Bohrmann, G., Dubé, T.E., Poole, F.G., 2003. Formation of modern and Paleozoic stratiform barite at cold methane seeps on continental margins. *Geology* 31 (10), 897–900.
- Trindade, R.I.F., Font, E., D'Aguerra-Filho, M.S., Nogueira, A.C.R., Riccomini, C., 2003. Low-latitude and multiple geomagnetic reversals in the Neoproterozoic Puga cap carbonate, Amazon craton. *Terra Nova* 15 (6), 441–446.
- Wing, B.A., 2013. A cold, hard look at ancient oxygen. *Proc. Natl. Acad. Sci.* 110 (36), 14514–14515.
- Wing, B.A., Halevy, I., 2014. Intracellular metabolite levels shape sulfur isotope fractionation during microbial sulfate respiration. *Proc. Natl. Acad. Sci.* 111 (51), 18116–18125.
- Wu, N., Farquhar, J., Strauss, H., Kim, S.T., Canfield, D.E., 2010. Evaluating the S-isotope fractionation associated with Phanerozoic pyrite burial. *Geochim. Cosmochim. Acta* 74 (7), 2053–2071.
- Yung, Y.L., DeMore, W.B., Pinto, J.P., 1991. Isotopic exchange between carbon dioxide and ozone via O (1D) in the stratosphere. *Geophys. Res. Lett.* 18 (1), 13–16.
- Yung, Y.L., Lee, A.Y., Irion, F.W., DeMore, W.B., Wen, J., 1997. Carbon dioxide in the atmosphere: isotopic exchange with ozone and its use as a tracer in the middle atmosphere. *J. Geophys. Res., Atmos.* 102 (D9), 10857–10866.
- Zhou, C., Bao, H., Peng, Y., Yuan, X., 2010. Timing the deposition of ^{17}O -depleted barite at the aftermath of Nantuo glacial meltdown in South China. *Geology* 38 (10), 903–906.